



**Statistical complexity of potential energy landscape as a dynamic signature of the glass transition**Dong Han,<sup>1,2</sup> Dan Wei <sup>1,2</sup> Peng-Hui Cao,<sup>3,4</sup> Yun-Jiang Wang <sup>1,2,\*</sup> and Lan-Hong Dai<sup>1,2,†</sup><sup>1</sup>State Key Laboratory of Nonlinear Mechanics, Institute of Mechanics, Chinese Academy of Sciences, Beijing 100190, China<sup>2</sup>School of Engineering Science, University of Chinese Academy of Sciences, Beijing 100049, China<sup>3</sup>Department of Mechanical and Aerospace Engineering, University of California, Irvine, California 92697, USA<sup>4</sup>Department of Materials Science and Engineering, University of California, Irvine, California 92697, USA

(Received 27 June 2019; revised manuscript received 12 January 2020; accepted 5 February 2020; published 18 February 2020)

Dynamic heterogeneity is an intrinsic characteristic of amorphous materials that is closely related to the mysterious glass transition. However, there is seldom an intuitive physical parameter characterizing the degree of dynamic heterogeneity and linking it quantitatively to the dynamic arrest phenomenon at the glass transition. Here, we propose a general theoretical protocol to explain the glass transition via a statistical parameter quantifying the dynamic heterogeneity of glass-forming systems. The parameter can be calculated using the concept of the Shannon information entropy associated with the variation in the activation barriers to local structural excitations on the underlying potential energy landscape, which can be explored extensively using the recently developed activation-relaxation technique in inherent structures spanning a wide range of configurational space. The concept is demonstrated successfully in a model of a prototypical glass-forming system  $\text{Cu}_{50}\text{Zr}_{50}$ . The Shannon entropy and statistical variation in the activation barriers are found to change dramatically at the glass-to-liquid transition and, therefore, can be treated as a novel signature of the glass transition, beyond the conventional thermodynamic indicators, such as the volume, potential energy, enthalpy, and heat capacity. The temperature-dependent Shannon entropy coincides with the evolution of the experimentally available stretching exponent during the glass-to-liquid transition and provides an intuitive explanation for the obscure decrease in dynamic heterogeneity from a metastable glass to an equilibrium liquid. Finally, possible relationships among structures, thermodynamics, and dynamics are discussed in terms of quantitative correlations among the structural Shannon entropy, excess total entropy, and dynamic Shannon entropy, respectively.

DOI: [10.1103/PhysRevB.101.064205](https://doi.org/10.1103/PhysRevB.101.064205)**I. INTRODUCTION**

The glass transition is a ubiquitous phenomenon in nature in which a liquid falls out of equilibrium as it is rapidly quenched to low temperatures at a sufficiently high cooling rate [1–4]. This phenomenon yields a disordered solid structure instead of the conventional crystals, which, in turn, leads to unique physical and mechanical functions [5,6]. Although the dynamics starts to slow at glass formation in the entire sample [7,8], the atomic structure is quite spatially inhomogeneous; both solidlike and liquidlike regimes are present [9–11] and have different mobilities where the viscosity spans timescales covering many orders of magnitude [12–14]. This is why appreciable dynamic heterogeneity is frequently observed in the relaxation, aging, and elastoplastic deformation of amorphous solids [14–18]. The well-known non-Arrhenius relaxation of highly viscous liquids and the underlying mechanism of the strong-to-fragile transition are also based on dynamic heterogeneity [12,13].

An empirical stretched exponential function in the form of the Kohlrausch-Williams-Watts (KWW) expression  $f(t) \sim$

$\exp[-(t/\tau_0)^{\beta_{\text{KWW}}}]$  is typically used to define the dynamic heterogeneity of a glass-forming system [14,18–23]. The system is usually investigated by tracing the temporal evolution of a specific response function  $f(t)$  involving, e.g., the stress, mean-squared displacement, and intermediate scattering function [19–21,24–26]. Here,  $\tau_0$  is a characteristic mean-field relaxation time.  $\beta_{\text{KWW}}$  is a stretching exponent that empirically quantifies the degree of nonexponentiality of a dynamic process, which can also serve as a qualitative indicator of the degree of dynamic heterogeneity. For a unique relaxation mechanism without any dynamic heterogeneity,  $\beta_{\text{KWW}} = 1$ . This is usually the case for the dynamics of an equilibrium liquid at high temperatures or plastic deformation of crystals, which is accommodated by a specific thermally activated microscopic mechanism, for instance, diffusion and dislocation motion [27,28]. However, this parameter can be only a small fraction of unity at low temperatures, indicating the existence of a wide spectrum of relaxation timescales in a deeply glassy state, which is representative of strong dynamic heterogeneity [14,18–21].

Although stretched exponential relaxation successfully explains many dynamic processes in glasses, such as stress relaxation [19,20,25], aging [23,24], and creep [29], there are few proposals for the physical foundation of this equation to date [22,29]. In particular, the attempt to link the degree

\*yjwang@imech.ac.cn

†lhldai@lnm.imech.ac.cn

of dynamic heterogeneity to the glass transition seems to be ambitious. On one hand, the difficulty lies in the lack of reasonable protocols to effectively compress all the timescales into one effective characteristic timescale in the framework of a generalized Maxwell viscoelastic model without exact topological information on the short-circuit relaxation channels [30]. On the other hand, accurate determination of individual relaxation timescales with distinct mechanisms is usually difficult because the data have to be extracted from a global response function via discretization or even continuous spectrum fitting with numerous fitting parameters, which usually involves a very large uncertainty [20,31,32].

In this paper, we address these issues by defining physically sound parameters for quantifying the degree of dynamic heterogeneity and associating the parameters with the glass transition. The parameters are deduced by performing statistical calculations on the activation barriers of local structural excitation in the inherent structures of a model glass former. In terms of the potential energy landscape (PEL), local atomic rearrangement corresponds to hoppings between neighboring potential energy minima that are separated by a saddle-point configuration, whose energy difference from that of the initial configuration defines an activation barrier for a local structural excitation event in the PEL [1,2,33–36]. The distribution of these activation barriers is a strong function of the inherent structure temperature and the cooling history (inherent structure inherited from a frozen configuration at a specific temperature). Tracing the evolution of the activation barrier distribution with temperature should be a straightforward way to see the variation in dynamic heterogeneity because dynamic features can be thoroughly expressed in terms of the degree of complexity of the PEL. Fortunately, the activation barriers can be extensively explored using the recently developed methods, such as the hybrid eigenvector-following approach [37,38], the dimer method [39], the gentlest ascent dynamics method [40], and the activation-relaxation technique (ART) [41], which can overcome the timescale limitation in conventional molecular dynamics (MD) simulations of the dynamics of amorphous solids [42,43]. As an open-ended method, ART is used due to its efficiency in randomly sampling a large number of events. ART and the hybrid eigenvector-following approaches could be unified in the same theoretical framework using the concept of the Krylov subspace. In ART, the Lanczos method finds the lowest eigenvalue in a Krylov subspace of increasing size, whereas the hybrid eigenvector-following approach searches in a smaller subspace spanned by the set of previous search directions [38]. Therefore, they are similar in some theoretical perspectives but a little different in operations. Here, we adopt ART since it facilitates exploration of large barriers that are inaccessible to normal MD simulations and, hence, can be used to explore a complete barrier spectrum in the inherent structures of glass-forming systems [44–50].

Here, a new concept, the Shannon information entropy [51], is introduced to characterize the variation of the activation barriers in terms of their spectra in different configurational spaces. This quantity clearly changes during the glass transition, in good agreement with experimental observations of the evolution of the stretching exponent  $\beta_{\text{KWW}}$  in the KWW equation [19]. Therefore, we provide a statistical

parameter that indicates the glass transition in terms of the dynamic heterogeneity extracted directly from the PEL. The non-Arrhenius average relaxation time can be clearly visualized after the statistical information on the nonequilibrium evolution of inherent structures in the PEL of a glass-forming system has been obtained [52,53].

## II. METHODOLOGY

The PEL of an extensively studied binary glass-forming system  $\text{Cu}_{50}\text{Zr}_{50}$  is sampled where the force field is described by a realistic many-body interacting embedded-atom method (EAM) potential [54]. There are 10 976 atoms in the model glass, which has dimensions of  $60 \times 60 \times 60 \text{ \AA}^3$ . The ART NOUVEAU (ARTN) software [41] implemented in the LAMMPS code [55] is adopted to obtain the force field and energetics of disordered structures at both the energy minimum and the saddle point as well as the image configurations between them. To trace the evolution of the spectrum of the activation barrier as a function of temperature, we quench the glass-forming system from its equilibrium liquid state at 2000 K to the deep glass state at 0 K at a constant cooling rate of  $10^{10} \text{ K/s}$  in the framework of an isothermal-isobaric ensemble [56]. The temperature is controlled by a Nosé-Hoover thermostat [57]. The MD time step is 2 fs. Periodic boundary conditions are applied in all three directions. During cooling, we take dozens of configuration fragments from the trajectory and bring them to their local energy minima using a conjugate gradient algorithm. The relaxed configurations, therefore, represent the inherent structures of the glass-forming liquid and glass at specific temperatures. The inherent structures are then input to ARTN to probe possible activation events.

To explore the activation barriers of local structural excitations, we choose and perturb a local cluster around a specific atom with a cutoff distance of  $3.95 \text{ \AA}$  (including nearest-neighbor atoms) in random directions with an initial perturbation displacement of  $0.10 \text{ \AA}$ . The increment is added stepwise at  $0.15\text{-}\text{\AA}$  intervals. When the smallest eigenvalue of the Hessian matrix becomes smaller than a critical value of  $-0.30 \text{ eV/\AA}$ , we bring the energy state to the saddle point along the weakest eigenvector direction using the Lanczos algorithm [58]. If the maximum force of any atom is below  $0.05 \text{ eV/\AA}$ , the configuration is assumed to converge on the saddle point. Every atom cluster is activated successfully 20 times, accounting for the statistics of the complexity of the high-dimensional configuration space of disordered materials. We explore as many as 219 520 possible events in the PEL that represent the dynamic heterogeneity because each event represents a local structural excitation with a very different incubation timescale. The calculations are reported in more detail in our previous work [59].

## III. RESULTS AND DISCUSSION

### A. Conventional identification of glass transition via thermodynamics

The most conventional way to determine the thermal glass transition temperature  $T_g$  during cooling from an equilibrium liquid is probably by examining the discontinuities in several thermodynamic parameters, which usually include

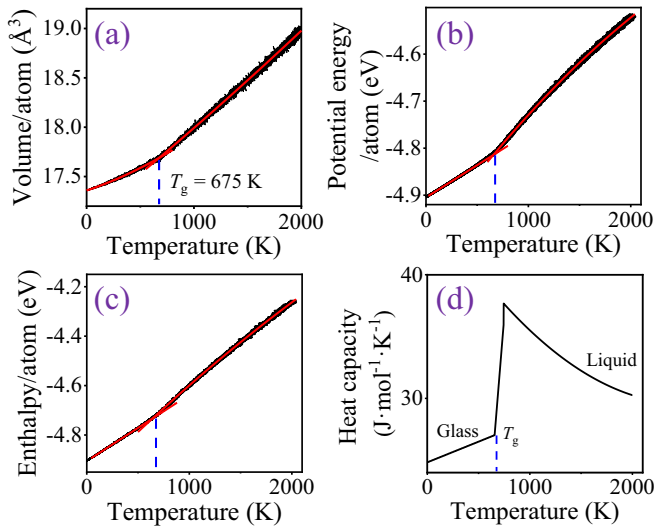


FIG. 1. Glass transition according to conventional thermodynamic parameters: (a) volume, (b) potential energy, (c) enthalpy per atom, and (d) specific heat capacity in the modeled  $\text{Cu}_{50}\text{Zr}_{50}$  glass-forming system. The glass transition temperature is consistently found to be 675 K.

the volume, potential energy, enthalpy, and heat capacity of a glass-forming system [12,60]. Following this strategy, in Figs. 1(a)–1(d), we demonstrate the temperature dependence of these quantities. They consistently yield  $T_g = 675$  K at a constant cooling rate of  $10^{10}$  K/s as performed in the present MD simulations. The calculated  $T_g$  is in agreement with the reported experimental data, e.g.,  $T_g = 651$  K in Ref. [60] and  $T_g = 679$  K in Ref. [61]. The red solid curves in Fig. 1 are the best nonlinear fits of the thermodynamic data on the MD cooling trajectory. All the kinks and discontinuities in these curves are distinct transition points indicating transitions in the thermodynamic phase. Note that the heat capacity shown in Fig. 1(d) is obtained by taking the derivative of the enthalpy [Fig. 1(c)] with respect to temperature.

Although these parameters are accurate indicators of the thermal glass transition, all the criteria are based on thermodynamics. The results lack direct dynamic information that is more directly related to the underlying mechanism of the glass transition, which is, in fact, a dynamic process. A question naturally arises regarding whether one can determine the glass transition in terms of purely dynamic characteristics, e.g., by examining the degree of complexity of the PEL. The solution not only explains the onset of dynamic heterogeneity after dynamic crossover with decreasing temperature, but also suggests a ubiquitous non-Arrhenius average relaxation time for the glass transition. In the following, we will attempt to supply the missing measurement of the glass transition from purely dynamic parameters.

## B. Spectrum of activation barrier

In this section, we address the issue of associating the glass transition with a physically meaningful dynamic quantity. This is performed by establishing a framework for quantitative characterization of the dynamic heterogeneity according to the complexity of the underlying PEL of a glass-forming

liquid [2,34,36], which can give the glass transition an explicit physical meaning. Figure 2 shows the histograms of the activation barriers  $\Delta Q$  for a wide range of inherent structures explored by ARTN. They are inherited from configurations frozen at different positions of the cooling history, which span the entire range from an equilibrium liquid to a metastable glass with supercooled states between them. It is not surprising to see a wide range of activation barrier distributions, which is attributed to the disordered nature of glasses and liquids. The present calculated spectra are in quantitative agreement with early calculations, such as those of Fan and co-workers [46–49] and Ding *et al.* [50]. The spectrum of the activation barrier is found to be highly temperature dependent as in the case of disordered materials prepared at different cooling rates [48,49]. Two basic relaxation modes generally appear in the distribution [48]. Mode I relaxation involves an exponentially decaying distribution function. It dominates the activation barriers in the supercooled liquid or liquid state at high temperatures. In this case, lower barriers are more common. Consequently, one has more possibility to note the percolation of high mobility regions in the glass-forming sample under external thermal or mechanical excitations. Therefore, the relaxation or deformation mode tends to exhibit cascade behavior over a large geometry [47]. Mode II relaxation involves a shifted Rayleigh distribution function. It is more likely to appear in glassy configurations. This type of distribution usually indicates a localized relaxation mode [47]. In this case, slowly mobile (rigid) regions are abundant in the sample. A solid skeleton that resists shear or thermal activation is easily formed [15]. The spatially sparse low-barrier regions (corresponding to the left tail of the barrier spectrum) are active within a typical laboratory timescale. This behavior usually excludes an extended relaxation mode in the deep glass configuration. However, the relaxation could be a localized feature at low temperatures, such as the usual phenomena of  $\beta$  relaxation [62,63] or shear transformation [64,65]. As the temperature decreases at the liquid-to-glass transition, a shift from a cascade to localized relaxation occurs. It also indicates the onset of dynamic heterogeneity, which is closely related to the glass transition.

Now, we quantitatively characterize the distribution of barriers, which will provide accurate information about the dynamic heterogeneity. For this purpose, we follow the proposal of Fan *et al.* in their recent work [48] in which the probability distribution function of the activation barriers is decomposed into two distinct modes, i.e.,

$$P(\Delta Q) = W \frac{1}{\varepsilon} \exp\left[-\frac{\Delta Q}{\varepsilon}\right] + W' \Delta Q \exp\left[-\frac{(\Delta Q - \mu)^2}{2\sigma^2}\right]. \quad (1)$$

The first term on the right-hand side of Eq. (1) represents mode I activation (cascade relaxation), whereas the second term represents mode II activation (localized relaxation). In the literature, a similar normal distribution or improved log-normal distribution has been assumed, which can predict the plasticity of metallic glasses reasonably well in the framework of thermal activation [66,67]. In Eq. (1), the parameter  $W$  is the amplitude of mode I, where  $1/\varepsilon$  is a decay constant.  $W'$  is the relative weight,  $\mu$  is the peak position, and  $\sigma$  is the scale

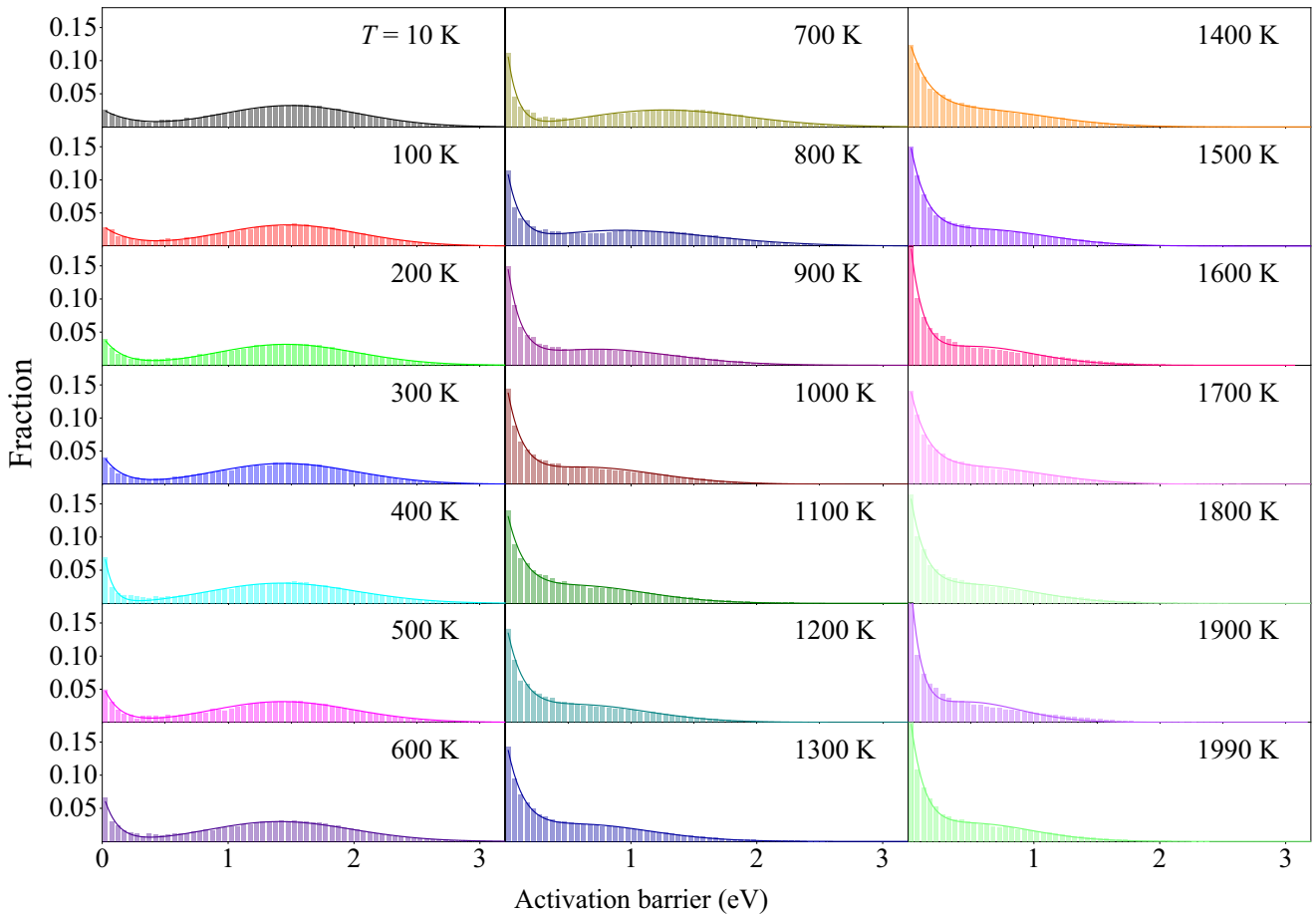


FIG. 2. Temperature-dependent histogram of activation barriers from the deep glassy state to the liquid state of  $\text{Cu}_{50}\text{Zr}_{50}$  glass formers. The distribution can be decomposed into two distinct modes. One is a shifted Rayleigh distribution representing local features of structural excitation of an amorphous solid. The other is an exponentially decaying model that is typical of nonlocal cascade deformation in a liquid. As the temperature increases above  $T_g = 675$  K, the deformation mode of the liquid gradually dominates the dynamics. The solid curves in the panels are nonlinear fits according to Eq. (1). The temperatures are those of inherent structures before the kinetic energy is removed.

parameter of mode II activation. The solid curves in Fig. 2 are the best nonlinear fits of the spectra of the activation barriers according to Eq. (1). The fittings are very satisfactory. They indicate that the assumed mixed distribution can capture the features of possible thermal structural excitation in the PEL reasonably well.

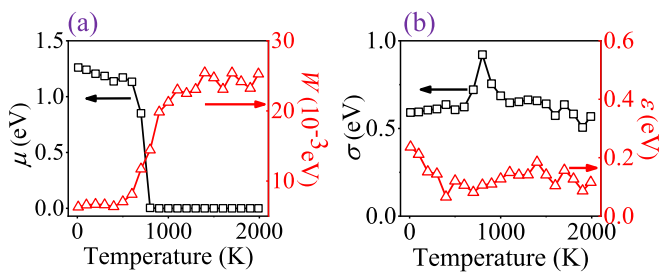


FIG. 3. Evolution of fitting parameters, (a)  $\mu$ ,  $W$  and (b)  $\sigma$ ,  $\epsilon$  in Eq. (1) for activation by modes I and II, respectively, as a function of the temperature of the inherent structures. The fits of the spectra shown in Fig. 2 are based on Eq. (1).

In Fig. 3, we plot the evolution of all the fitting parameters except  $W'$  as a function of configuration temperature because  $W'$  can actually be determined from the normalized condition once the form of the distribution is fixed. As the temperature increases from 10 to 1990 K,  $W$  starts to increase substantially at the glass transition temperature ( $T_g = 675$  K). However,  $W$  remains almost zero in the glassy state. This means that mode I activation dominates the dynamics after the glass transition. However, it always occurs over the entire temperature range at an almost constant decay rate as indicated by the constant value of  $\epsilon = (0.14 \pm 0.04)$  eV shown in Fig. 3(b). It corresponds to the left tail of the barrier distribution even at low temperatures as shown in Fig. 2. This represents the so-called liquid region frozen in the solid glass state, which is irrelevant to the inherent structure temperature. Mode II activation generally dominates the glassy dynamics at low temperatures. Because mode II activation spans a wide range of activation barriers, there should be obvious dynamic heterogeneity [6]. An interesting observation is that  $\mu$  for mode II becomes slightly smaller with increasing temperature before the glass transition. This may suggest that the effective activation barrier becomes smaller, and thermal activation is easily

triggered. However, the range of the mode II activation energy is almost independent of the temperature of the inherent structure. Moreover, the scale parameter remains nearly unchanged at  $\sigma = (0.64 \pm 0.08)$  eV, except for a sudden increase at the glass transition point, which may be a numerical error due to the dramatic shift in  $\mu$ . Here, the magnitude of  $\sigma$  is in agreement with the value of 0.49 eV reported in the literature [48]. In brief, the finding of the transition from the mode I to the mode II distribution at the liquid-to-glass transition indicates a shift in the mechanism from cascade to localized relaxation or from the liquid dynamics to the glassy dynamics during cooling. It also explains the divergence of the main ( $\alpha$ ) and secondary ( $\beta$ ) relaxation at the mode-coupling critical temperature [2,6]. Although we demonstrate the transition in terms of a change in the inherent structure temperature, it resembles the transition of the relaxation modes if one changes the cooling rate in the glass sample preparation process [47,49].

### C. Spatial characteristics of the potential energy landscape

The hypothesis of a relaxation mode transition observed in the spectra of activation barriers can be further confirmed and explained by the topological characteristics. To this end, we plot the heat map of an activation barrier in a slice perpendicular to the  $z$  direction as shown in Fig. 4. The thickness of the slice is 3.95 Å, which corresponds to the first minimum of the radial distribution function. The activation barrier is, therefore, coarse grained at this thickness. The spatial characteristics represent two distinct scenarios of possible structural excitation for either the glassy state at 100 K as shown in Fig. 4(a) or the liquid state at 1990 K as shown in Fig. 4(b). For a convenient laboratory observation timescale of  $\tau = 10^2$  s, the critical activation barrier for this local structural excitation is  $\Delta Q_c = k_B T \ln(\tau/\tau_0) \approx 37k_B T$ , where  $k_B$  is the Boltzmann constant. As a first approximation, here, we assume a relaxation time prefactor on the order of  $\tau_0 = 10^{-14}$  s [13,53]. This barrier is approximately 0.95 eV at ambient temperature  $T = 300$  K. From the barrier heat map shown in Fig. 4(a), one can deduce that the activated structural arrangement should be localized (where the barrier region is smaller than 0.95 eV). It is evident that the low-barrier regions in the glass are highly localized as exemplified by the local region indicated by an arrow in Fig. 4(a). The dimensions of this possible local structural excitation are of subnanometer order. The local nature of structural excitation in the glass is consistent with the common understanding of secondary  $\beta$  relaxation [62,63] or shear transformation in terms of the plastic deformation zone [64,65]. The size of the low-barrier regime is also consistent with the consensus that a shear transformation event involves nanoscale rearrangements of several tens of atoms [64,68].

However, the incubation timescale of an event at high temperature should be much shorter, possibly even comparable to the order of the phonon lifetime under extreme conditions. In this case, the critical activation barrier  $\Delta Q_c = k_B T \ln(\tau_{\text{phonon}}/\tau_0)$ , should be extremely small. Then the landscape-dominated relaxation mechanism will be replaced by diffusive viscous flow once the thermal energy is high enough to explore a large fraction or even all of the shallow

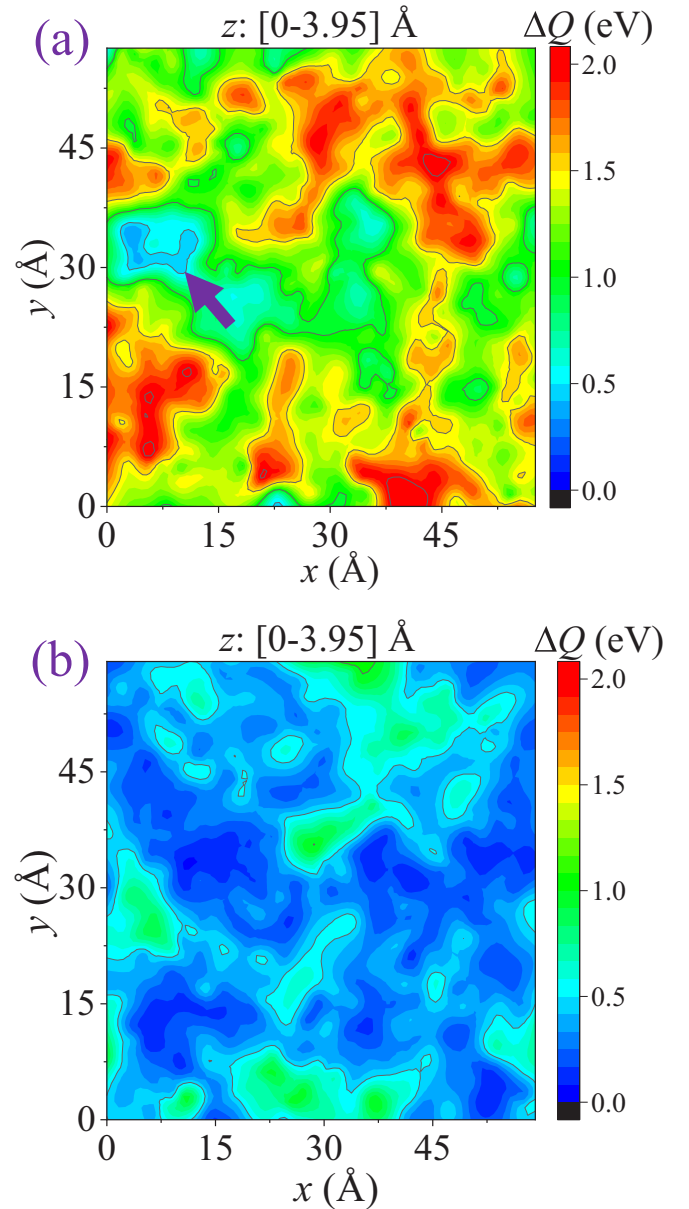


FIG. 4. Spatial features of activation barriers in (a) deep glassy state at 100 K and (b) equilibrium liquid state at 1990 K. The heat maps demonstrate clearly that the excitation is localized in the glass but nonlocal in the liquid, supporting the scenario of the glass transition as a consequence of a change in the relaxation mode from primary ( $\alpha$ ) relaxation to secondary ( $\beta$ ) relaxation with decreasing temperature. The arrow in (a) indicates a location of possible  $\beta$  relaxation that is a feature of a low-energy barrier. The  $xy$  plane is a coarse-grained slice with a thickness of 3.95 Å perpendicular to the paper plane.

energy minima of the PEL. As shown in Fig. 4(b), the low-barrier regions in the inherent structure of a liquid are much more extended. The highly mobile regimes tend to percolate through the entire sample, which is ready to be triggered into a large relaxation mode or extended deformation. The scenario is in agreement with the deduction from a power-law scaling distribution of the activation barrier in the inherent structure of an unstable glass-forming liquid that is instantly

quenched from an equilibrium liquid state [47]. Therefore, we conceived a basic idea of enhanced dynamic heterogeneity from the liquid to the glass, based on the evolution of the spatial characteristics of the activation barrier. The patterns of the activation barrier also support the scenario of a reduction in the static configuration correlation at the liquid-to-glass transition [16,69,70].

#### D. Statistical complexity of the PEL and glass transition

Having qualitatively explained the evolution of the activation barrier spectrum, we now provide a general strategy to quantify the degree of dynamic heterogeneity of a glass-forming system on the basis of the complexity of the hyperdimensional surface where the configuration remains at the relative position of the PEL. Because the distribution of activation barriers in Fig. 2 characterizes a wide variety of timescales in the dynamics, if we can quantitatively measure the variation in these activation barriers, then, we may have a physically sound number that reveals the dynamic heterogeneity. In the literature, a set of parameters characterizing the level of frustration of the energy landscape have been proposed based on the topological features of PEL, and, meanwhile, a novel Shannon entropy concept defined with the information of local energy minima in the equilibrium state is also applied to quantify frustration in glassy systems [71,72]. Inspired by those concepts, here, we adopt Shannon entropy to measure the complexity of the activation barriers (the shape of the spectrum) as well as multiplicity of local short-range Voronoi structures [73], which yield dynamic and structural Shannon entropy, respectively. Here, we apply the concept of Shannon entropy to characterize the variation in the activation barriers, such as those shown in Fig. 2. Because the distribution functions are continuous, the dynamic Shannon entropy is defined as

$$S_{\text{Shannon}}(T) = - \int_0^{\infty} P(\Delta Q) \ln[P(\Delta Q)] d\Delta Q. \quad (2)$$

Here,  $P(\Delta Q)$  is a normalized probability distribution function of an activation barrier. In practice, the entropy can be calculated numerically as  $S_{\text{Shannon}}(T) = - \sum_i P_i(T) \ln P_i(T)$  after discretization of the spectra into a finite number  $i$  of bins of appropriate width. Because the distribution is temperature dependent, the variation in the barriers and, thus, the complexity of the PEL are naturally related to the temperature. This novel parameter will be shown to be not only a number indicative of the dynamic heterogeneity, but also an intuitive signature of the glass transition. Finally, we note that the present definition of the Shannon entropy is not equivalent to any specific form of physical entropy that we are familiar with in statistical mechanics. It is only a statistical number facilitating quantitative measurement of the degree of complexity of the dynamics, which usually involves multiple timescales.

On the other hand, the statistical variation in the activation barriers (or dynamic diversity) obtained from the spectrum is defined according to the dynamic Shannon entropy,

$$D_{\text{barrier}} = \exp(S_{\text{Shannon}}). \quad (3)$$

The dynamic diversity  $D_{\text{barrier}}$  could be an intuitive number indicating how hierarchical the dynamics of a glass-forming

system is. For a single activation barrier, there is no dynamic heterogeneity. In our framework, the situation has  $S_{\text{Shannon}} = 0$  and  $D_{\text{barrier}} = 1$ . Then, the timescale of the dynamics can be well described by the conventional Arrhenius equation  $\tau \propto \exp(\Delta Q/k_B T)$  with  $\beta_{\text{KWW}} = 1$ . This describes the dynamics of a strong substance, such as the everyday window glass  $\text{SiO}_2$  [2,12] as well as a unique thermally activated plastic mechanism in crystalline materials [27,28]. However, there will be a wide distribution of the constituent timescales or activation barriers for a fragile glass [2,12]. In this case, the dynamic Shannon entropy will be a positive number with the diversity parameter  $D_{\text{barrier}} \gg 1$ . This corresponds to the stretched exponential dynamics with  $0 < \beta_{\text{KWW}} \ll 1$ . As a result, one may anticipate that the variation in the parameters  $S_{\text{Shannon}}$  and  $D_{\text{barrier}}$  could be in accord with that of the conventional  $\beta_{\text{KWW}}$  parameter in the KWW function and could explain the underlying mechanism of dynamic heterogeneity in disordered materials.

Now, we apply the new concepts to  $\text{Cu}_{50}\text{Zr}_{50}$  glass formers. The calculated dynamic Shannon entropy describing the distribution of activation barriers and the barrier diversity parameter are shown in Figs. 5(a) and 5(b), respectively. The most significant feature is that both the dynamic Shannon entropy and the dynamic diversity start to decrease dramatically with increasing temperature at the glass transition. This means that the proposed parameters are effective for characterizing the degree of dynamic heterogeneity. It is easier to note that the degree of dynamic heterogeneity changes noticeably from the temperature derivatives of dynamic Shannon entropy and dynamic diversity as shown in Figs. 6(a) and 6(b), respectively. Both of them are obtained by performing nonlinear fitting of the original data shown in Figs. 5(a) and 5(b). There is an apparent valley around the glass transition in the two curves of Fig. 6, which denotes an anomaly in the rate of change in dynamic heterogeneity from glass to liquid. They can be notable dynamic signatures of the glass transition in addition to the conventional thermodynamic criteria. In the inset of Fig. 5(a), we also provide a reference for comparison, which is the evolution of the stretching exponent  $\beta_{\text{KWW}}$  in the KWW equation describing the decay of stress in a stress relaxation experiment [19]. In that protocol, the hidden temperature-dependent evolution of the relaxation mode during the glass-to-liquid transition was successfully revealed by tracking  $\beta_{\text{KWW}}$ . Thus, the stretched exponent could be used to calibrate the proposed statistical parameters of the activation barrier. Because the KWW equation is a mean-field description of the hierarchical dynamics, the synchronous variation in  $S_{\text{Shannon}}$  and  $\beta_{\text{KWW}}$  should imply that the former is also a good physical parameter measuring the degree of dynamic heterogeneity. More specifically, once the stretching exponent increases from  $\beta_{\text{KWW}} \simeq 0.5$  to  $\beta_{\text{KWW}} \simeq 1$  at the glass-to-liquid transition, the dynamic heterogeneity gradually decreases. Simultaneously, the dynamic Shannon entropy changes from a plateau  $S_{\text{Shannon}} \simeq 3.7$  at low temperatures to another plateau  $S_{\text{Shannon}} \simeq 3$  at high temperatures.

In terms of the variation in the activation barriers or the dynamic diversity as shown in Fig. 5(b), the parameter  $D_{\text{barrier}}$  also changes dramatically at the glass-to-liquid transition. After the glass transition, this parameter changes from  $D_{\text{barrier}} \simeq 50$  to  $D_{\text{barrier}} \simeq 25$ . For a first approximation,

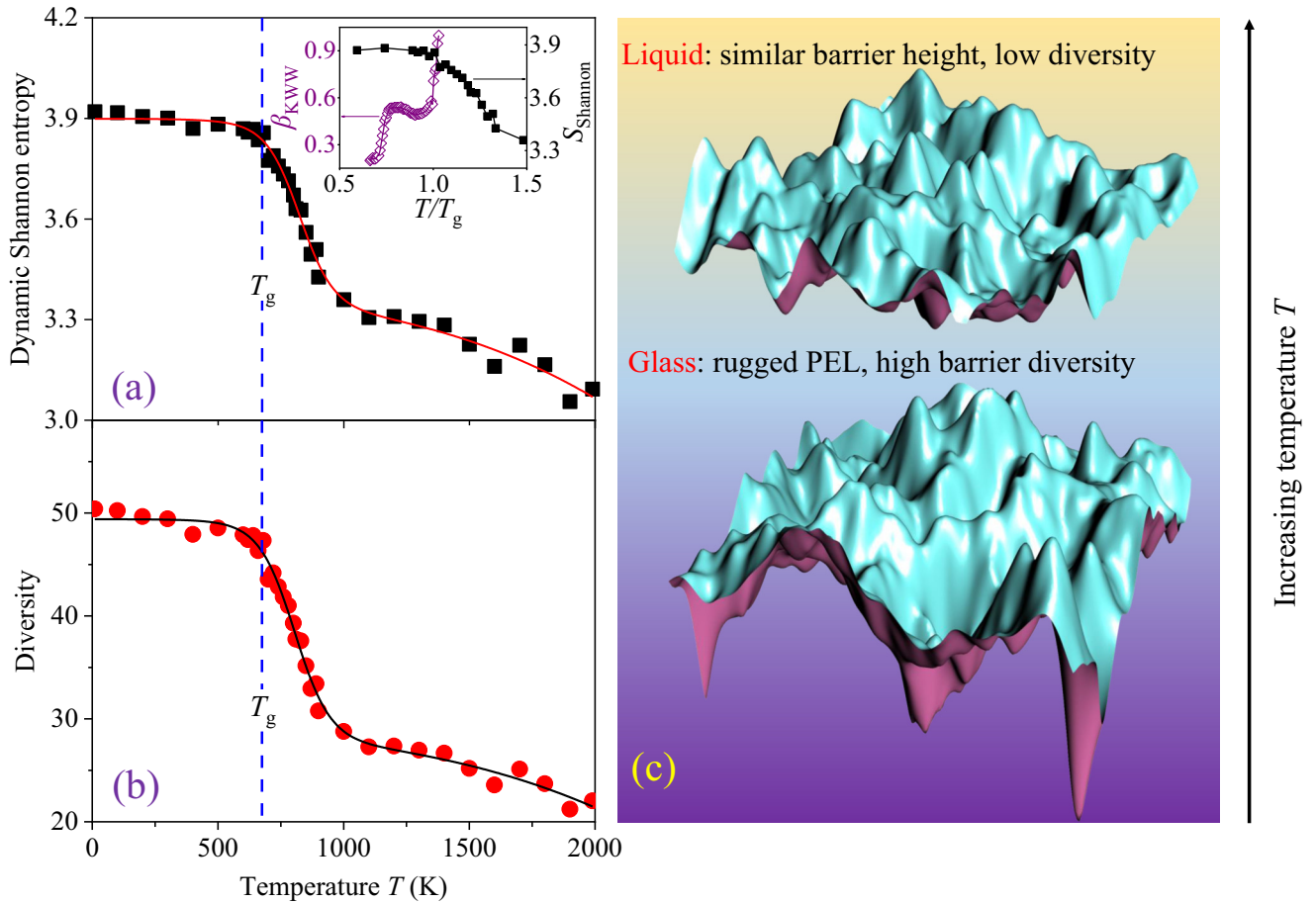


FIG. 5. Glass transition described by dynamic Shannon entropy and variation in the activation barriers. (a) Dynamic Shannon entropy of activation barriers as a function of temperature, which decreases dramatically at the glass-to-liquid transition. The inset provides a direct comparison with the experimentally available stretching exponent  $\beta_{\text{KWW}}$  in the KWW equation, which is an empirical parameter indicating the degree of dynamic heterogeneity. (b) Dynamic variation in the activation barriers, which decreases sharply after the glass-to-liquid transition, also indicating a decrease in the complexity of the potential energy landscape. The vertical dashed lines in (a) and (b) indicate the positions of the glass transition temperature. The solid curves in (a) and (b) are nonlinear fits of data points. (c) Schematic of the complexity of the PEL in the liquid and glass, respectively. Dense low-energy minima appear at similar depths in the PEL of the liquid, whereas sparse, large, and hierarchically arranged energy basins are typical of the topology of the PEL of the glass.

one can imagine that there are approximately 50 dashpots with distinct relaxation timescales in a generalized Maxwell model [20]. However, the number of dashpots decreases significantly which evolves to be only half numbers after the glass-to-liquid transition. It can serve as an intuitive physical interpretation of the puzzling reduction in the degree of dynamic heterogeneity with increasing temperature at the glass transition [19]. As demonstrated by the cartoon shown in Fig. 5(c), small dense energy basins appear in the PEL of the liquid. However, the activation barriers are of similar magnitude. All the activation barriers tend to move to the left tails of the spectra; see Fig. 2. Consequently, the low activation barriers dominate the distribution, resulting in less dynamic diversity and a small value of  $D_{\text{barrier}}$ . However, the energy minima in the PEL of the glass are sparse and deep with a strongly hierarchical distribution. Thus, the activation barrier distribution is wide. It is the physical foundation of the underlying large  $D_{\text{barrier}}$  as well as the high degree of dynamic heterogeneity in the glass. This scenario and quantification

of the PEL may also shed light on the widespread onset of non-Arrhenius relaxation and the dynamic arrest phenomenon in a wider variety of glass-forming systems as extensively discussed in the literature [12,52,53,74].

However, the dynamics is not only related to the spectrum of barriers, but also depends on the connectivity and organization of the underlying PEL, i.e., its topology. It is well known that a superstructure, namely, a metabasin constituted by a set of basins, emerges naturally in PEL as suggested in the literature [75–80]. As a way to describe the general shape and overall connectivity in the PEL, disconnectivity graphs [81,82], i.e., the one-dimensional projection of the  $3N$ -dimensional PEL, are frequently used to visualize topological features of a multidimensional PEL. The way maps the configuration space into samples of pathways linking multiple local energy minima via transition states (energy barriers or saddle points). On one hand, a vertex of the disconnectivity graph indicates a saddle point, and each branch terminates at a local energy minimum along its vertical axis (potential

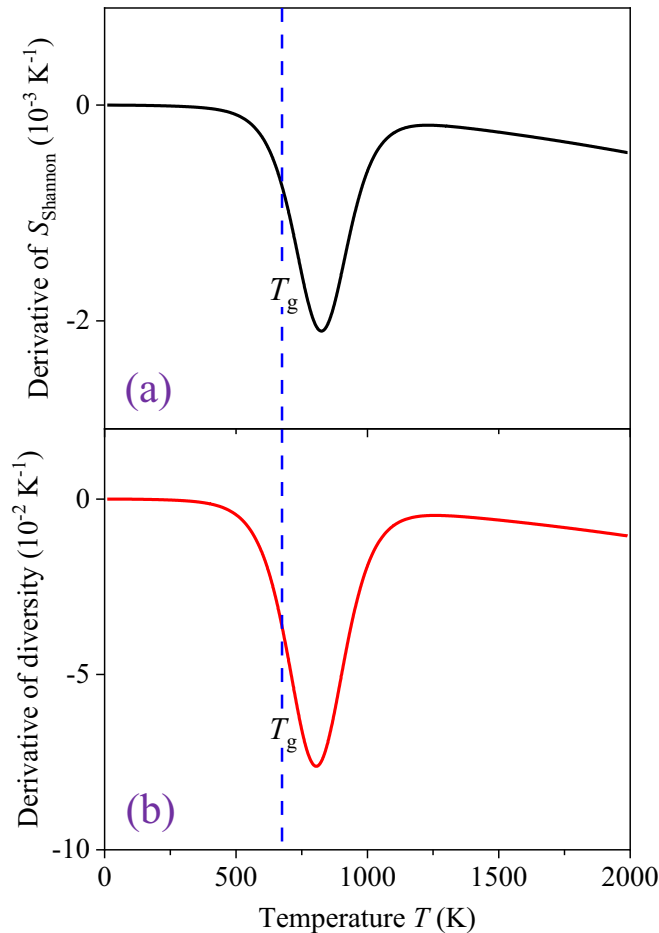


FIG. 6. The temperature derivatives of (a) dynamic Shannon entropy and (b) dynamic diversity, which are calculated based on the plot in Figs. 5(a) and 5(b).

energy). On the other hand, each single point stands for a superbasin including one or more daughter superbasins [83]. Recently, the temporal disconnectivity graph was developed in a binary Lennard-Jones glassy system, which can describe the temporal evolution of metabasins when they consolidate with time to form even larger metametabasins [80].

Here, to complement the schematic of the PEL as shown in Fig. 5(c), two representative disconnectivity graphs are demonstrated in Figs. 7(a) and 7(b), respectively. One is for an equilibrium liquid state at an inherent structure of 1990 K, and the other is for a deep glassy state at an inherent structure of 100 K. Both graphs consist of 2900 successive local activation events starting from a local energy basin, which enables sufficient sampling of possible configurations. The complex connectivity topology of the trajectories resembles the results demonstrated in different disorder systems in the literature [84–88]. In Fig. 7(a), the overall potential well depth is about 0.008 eV per atom. Various local minima sampled are densely distributed in a local space and most of the activation barriers are low. Moreover, the small barriers are of similar height, indicating less multiplicity of relaxation times is associated with less dynamic heterogeneity in the equilibrium liquid state. The profile for the equilibrium liquid state may

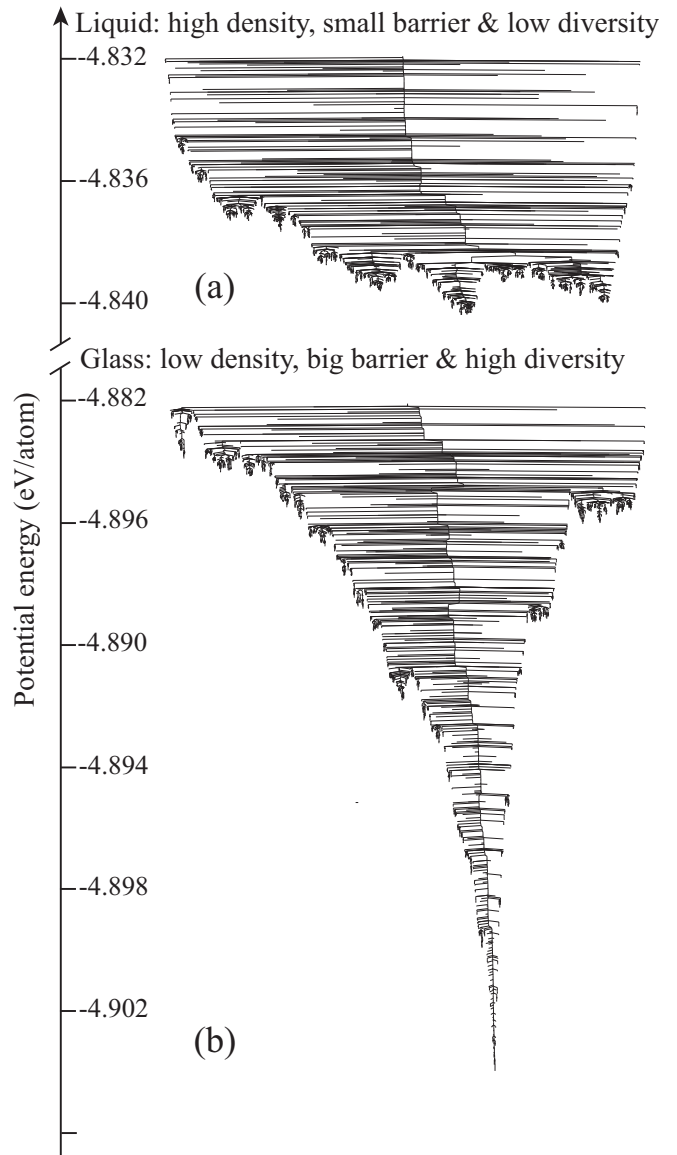


FIG. 7. Disconnectivity graphs for (a) the equilibrium liquid state at 1990 K and (b) the deep glassy state at 100 K, respectively. Each graph consists of 2900 successive activation events starting from a local energy basin representing a specific inherent configuration.

resemble that of a banyan-tree topology with relatively small fluctuations in depth of the local minima [89]. However, once starting from a deep glass state as shown in Fig. 7(b), extremely deep local basins locate at the depth of about 0.022 eV per atom. The graph corresponds to a palm-tree motif which owns a well-defined global minimum and relatively small downhill barriers [89]. The main branch indicates a metabasin which requires extremely numerous activation events to climb the large mountain. Many minima are scattered on the narrow fragment of the PEL. The activation barriers are relatively large with high diversity, implying enhanced dynamic heterogeneity in the glass state. One may anticipate that the topology of the top of the glass disconnectivity graph will be similar to that of the bottom of the liquid disconnectivity



graph, once the potential energy levels are compared to each other after exhausted exploration. Therefore, the scenarios from the disconnectivity graphs inosculate basically with our illustrations on the cartoon as shown in Fig. 5(c).

### E. Possible relationship between dynamics and structure

Dynamic features are typically thought to have deep origins in the structures of glasses and liquids [59,70,73,90]. To reveal the possible structural causes of the evolution of dynamic heterogeneity that accommodates the glass transition, we also examine the statistics of the distribution of Voronoi polyhedra in multiple inherent structures of a  $\text{Cu}_{50}\text{Zr}_{50}$  glass-forming liquid. The statistics of the structure is analogous with that obtained for the dynamics using the same concept of the Shannon information entropy and the variation in the activation barriers as shown in Eqs. (2) and (3). The only difference is that the distribution of activation barriers in the dynamics is replaced with that of the Voronoi polyhedra in the structural analysis. The idea has been shown to be very effective for characterizing the multiplicity of local structures in two model glass-forming binary atomic alloys, i.e.,  $\text{Cu}_{50}\text{Zr}_{50}$  as described by the EAM and a Lennard-Jones  $A_{80}B_{20}$  mixture [73]. First, in a specific inherent structure of a disordered configuration, we label each atom according to its Voronoi environment with a unique four-digit index  $\langle n_3, n_4, n_5, n_6 \rangle$ , where  $n_i$  is the number of faces with  $i$  edges [91–93]. Then, we obtain the statistics of the fraction of specific Voronoi polyhedra and extract the entire spectrum of the local structure distribution, which usually includes more than several hundreds of species of short-range structures. When the distribution of the Voronoi structures is available, we calculate the structural Shannon entropy as defined in Eq. (2), i.e., the value calculated numerically as  $S_{\text{Shannon}}(T) = -\sum_i P_i(T) \ln P_i(T)$  is then the fraction of a specific Voronoi polyhedron. By using this strategy, the structural diversity can be further quantified in terms of the structural Shannon entropy using Eq. (3).

The calculated structural Shannon entropy and structural diversity are plotted against the dynamic Shannon entropy and dynamic diversity in Fig. 8. Although the dynamic features are strongly correlated with the structural features, the general trend is that the dynamic diversity (or entropy) decreases with increasing structural diversity (or entropy). In other words, once the dynamic heterogeneity decreases at the glass-to-liquid transition, local disordered structures become more abundant. This correlation seems to be obscure, but it, indeed, can be explained by the change in structures. In the deep glassy state, the structural and dynamic features are confined well in a regime defined by the boundary between the glass and liquid as indicated by the horizontal dashed lines in Fig. 8. The dynamic Shannon entropy fluctuates about  $\sim 3.9$ , whereas the structural entropy is stable at  $\sim 4.55$ . The data for glass correspond to a dynamic diversity of  $\sim 50$  and structural diversity of  $\sim 95$ . After the glass-to-liquid transition occurs, the dynamic and structural features change substantially. This is because more configurational space can be explored for a liquid than for a glass [2]. After the glass transition, an increasing number of stable Voronoi structures are broken, producing more structural diversity with fewer stable local

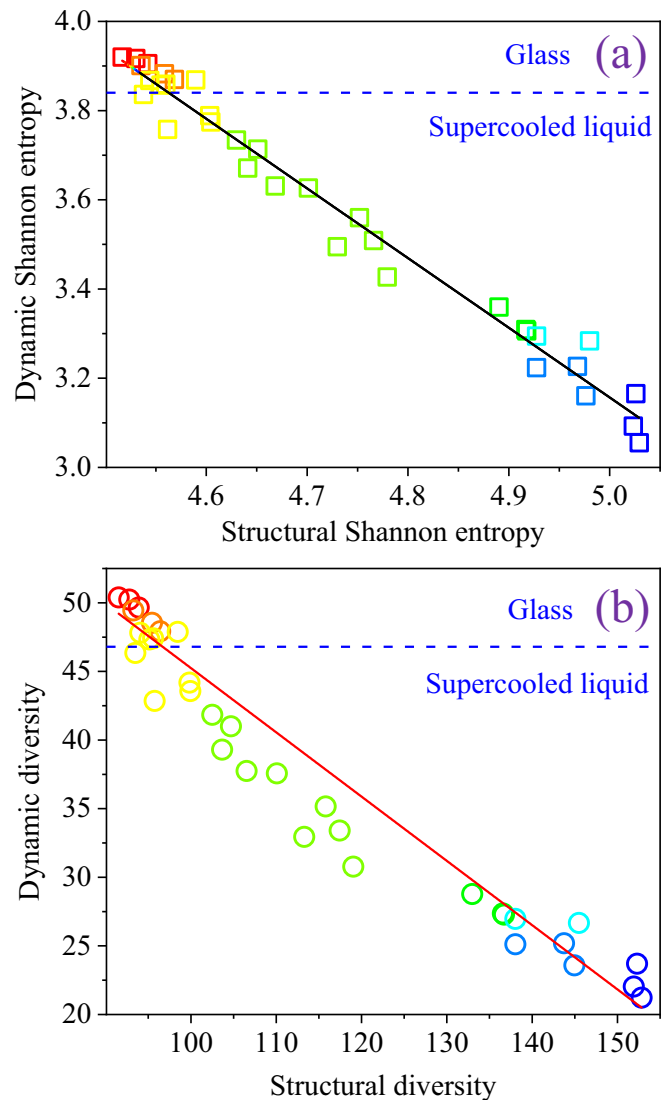


FIG. 8. Relationships between structural and dynamic heterogeneity in a  $\text{Cu}_{50}\text{Zr}_{50}$  glass-forming system. (a) Relationship between dynamic Shannon entropy and structural Shannon entropy. (b) Relationship between dynamic diversity and structural diversity. The solid lines represent apparent linear fits, which serve as guides for the eyes. The horizontal dashed lines are the boundaries between the glass and the supercooled liquid. The symbols are colored by the magnitudes of the temperatures of their inherent structures, starting with red for 10 K, and ending with blue for 1990 K, respectively.

structures. However, the newly generated structures resulting from the glass transition have low activation barriers as demonstrated by the evolution of the distribution shown in Fig. 2. With increasing temperature, the peak in the left tail of the activation barrier increases, whereas the central peak gradually disappears. Consequently, the barrier distribution becomes less uniform in the liquid state, i.e., the low-energy barrier events dominate the liquid dynamics. Simultaneously, the dynamic diversity and dynamic Shannon entropy decrease with this increase in the diversity or Shannon entropy of local structures. The scenario corresponds to the decrease in dynamic heterogeneity as indicated by the increase in the

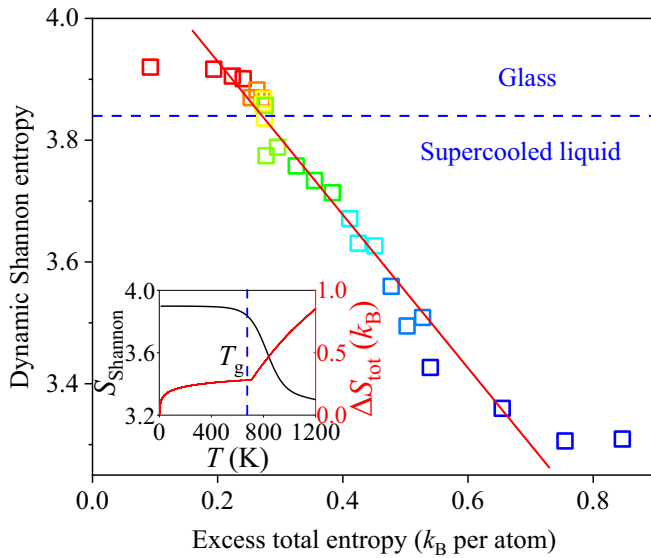


FIG. 9. Connection between the excess total entropy (thermodynamic entropy) and dynamic Shannon entropy in the  $\text{Cu}_{50}\text{Zr}_{50}$  glass-forming system. The solid line represents an apparent linear fit, which serves as guide for the eyes. The horizontal dashed lines are the boundaries between the glass and the supercooled liquid. The symbols are colored by the magnitudes of the temperatures of their inherent structures, starting with red for 10 K, and ending with blue for 1200 K, respectively. The inset shows how the dynamic Shannon entropy and excess total entropy change with temperature.

KWW stretching exponent  $\beta_{\text{KWW}}$ , which was observed in the stress relaxation experiment performed by Wang *et al.* [19]. Therefore, a preliminary link between the dynamics and the structure has been revealed using the newly defined Shannon entropy and diversity of both the activation barriers and Voronoi structures.

#### F. Connection between thermodynamic entropy and dynamic Shannon entropy

The Kauzmann paradox [94] and the success of the Adam-Gibbs entropic scenario [95] to some degree have suggested that the nature of glass transition should be based on both thermodynamics and dynamics [13]. Therefore, it is vital to understand the correlation between thermodynamics and dynamics in terms of the thermodynamic entropy and the proposed Shannon information entropy in the present paper. Aiming at clarifying the relationship, total entropy of the glass-forming system is obtained in our previous work [96]. It is performed by thermodynamic integration after heating a glass to its liquid counterpart, i.e.,  $S_{\text{tot}} = \int_0^T \frac{dQ}{T}$  within an isothermal-isobaric ensemble. Here,  $T$  is temperature, and  $Q$  is the absorption heat. Therefore, the excess total entropy  $\Delta S_{\text{tot}}$  of glass and liquid over crystal is defined as  $\Delta S_{\text{tot}} = S_{\text{tot}}^{\text{glass}} - S_{\text{tot}}^{\text{xtal}}$ .

As shown in the inset of Fig. 9, we provide a direct comparison of the dynamic Shannon entropy with the excess total entropy in the system. It is evident that the glass transition occurs at about 675 K at which entropies change dramatically.

To further clarify their possible relationship, the excess total entropy is plotted against the dynamic Shannon entropy in Fig. 9. In most cases, the dynamic entropy is strongly correlated with the thermodynamic entropy. A general trend is that the dynamic Shannon entropy decreases with increasing excess total entropy, i.e., thermodynamic entropy. A possible mechanism behind the phenomenon may be explained by combining Figs. 8 and 9. The structural diversity (hence entropy) increases as thermodynamic entropy increases (mainly from configurational entropy as demonstrated in Ref. [60]), which leads to reduction in dynamic diversity.

#### IV. CONCLUDING REMARKS

A new concept of dynamic heterogeneity is proposed using the Shannon information entropy to describe the variation in the activation barriers under local structural excitations in disordered solids and is demonstrated successfully in the underlying PEL of a model CuZr glass-forming system. The activation barriers are explored extensively by the well-established ARTN method, and the activation barrier spectra over a wide temperature range in configurational space are calculated for the glass-forming system. On the basis of the spectra, a statistical description of the dynamic diversity is built on the extracted dynamic Shannon entropy. Both the dynamic Shannon entropy and the dynamic diversity can quantitatively characterize the degree of dynamic heterogeneity. They both decrease dramatically at the glass-to-liquid transition, and, therefore, they can serve as intuitive numerical dynamic signatures of the general glass transition phenomenon. The validity of the parameters for characterizing the glass transition is calibrated by the commonly adopted stretching exponent of the KWW function, which can be extracted by a stress relaxation experiment. Although the demonstration is applied in an EAM model of a CuZr system, the method is expected to be generalized to evaluate the dynamic heterogeneity of other disordered materials if the activation barrier spectrum can be extracted from either atomistic simulations or experiments, such as creep, stress relaxation, and dynamic mechanical analyses.

Afterwards, a preliminary relationship between the dynamics and the structure is revealed by correlating the defined dynamic diversity (or entropy) of the activation barriers to the structural diversity (or entropy) of the Voronoi structures. The increase in less-stable Voronoi polyhedra with low-energy barriers enhances the uniformity of the activation barrier at the liquid state and, consequently, diminishes the dynamic Shannon entropy and dynamic heterogeneity. Finally, a possible relationship between the dynamics and the thermodynamics is established by relating the proposed dynamic Shannon entropy and excess total entropy of the glass-forming system. The observed correlation might connect two fundamental but important concepts in glass transition models: the Adam-Gibbs entropic scenario [95] and the PEL perspective [2,34–36]. Our strategy may pave the way to a complete explanation of the general glass transition phenomenon. It also provides hints to the solution of the long-standing scientific problem of understanding the non-Arrhenius temperature dependence of the relaxation time in glass-forming liquids [52,53].

## ACKNOWLEDGMENTS

We acknowledge financial support from the National Key Research and Development Program of China (Grants No. 2017YFB0701502 and No. 2017YFB0702003), the NSFC (Grants No. 11672299 and No. 11790292), the Strategic Priority Research Program (Grant No. XDB22040303), the Key Research Program of Frontier Sciences (Grant No. QYZDJSSW-JSC011), and the Youth Innovation Promotion Association of Chinese Academy of Sciences (Grant No. 2017025).

## APPENDIX: ESTIMATION OF NUMERICAL ERROR IN DYNAMIC SHANNON ENTROPY

To reduce the impact of insufficient sampling of possible configurations, we prepare another four (five in total) statistically independent binary  $\text{Cu}_{50}\text{Zr}_{50}$  glass-forming liquid systems for Shannon entropy as shown in Fig. 10. Here, we perform the ensemble average of dynamic Shannon entropy on configurations at three characteristic temperatures, i.e., 10, 700, and 1990 K. It is evident that each standard deviation of the entropy is less than 0.06, which is trivial compared to the average value of the five independent inherent structures. Therefore, the calculated Shannon entropy is reliable with reasonable numerical errors.

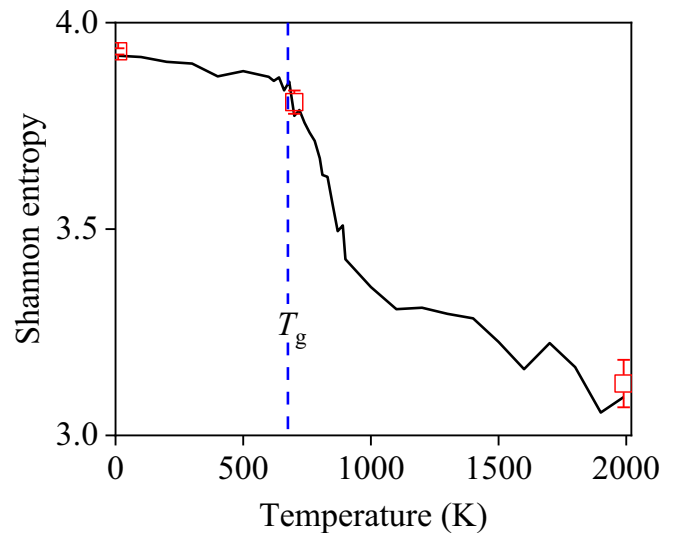


FIG. 10. Ensemble average of Shannon entropy at three characteristic temperatures. The solid line indicates the dependence of Shannon entropy on temperature. Each data point is an average of five independent inherent structures. The error bars stand for the standard deviation of the entropy in five statistically independent configurations.

- [1] S. Sastry, P. G. Debenedetti, and F. H. Stillinger, Signatures of distinct dynamical regimes in the energy landscape of a glass-forming liquid, *Nature (London)* **393**, 554 (1998).
- [2] P. G. Debenedetti and F. H. Stillinger, Supercooled liquids and the glass transition, *Nature (London)* **410**, 259 (2001).
- [3] J. C. Dyre, Colloquium: The glass transition and elastic models of glass-forming liquids, *Rev. Mod. Phys.* **78**, 953 (2006).
- [4] J. S. Langer, Theories of glass formation and the glass transition, *Rep. Prog. Phys.* **77**, 042501 (2014).
- [5] J. C. Qiao, Q. Wang, J. M. Pelletier, H. Kato, R. Casalini, D. Crespo, E. Pineda, Y. Yao, and Y. Yang, Structural heterogeneities and mechanical behavior of amorphous alloys, *Prog. Mater. Sci.* **104**, 250 (2019).
- [6] W. H. Wang, Dynamic relaxations and relaxation-property relationships in metallic glasses, *Prog. Mater. Sci.* **106**, 100561 (2019).
- [7] C. P. Royall, S. R. Williams, T. Ohtsuka, and H. Tanaka, Direct observation of a local structural mechanism for dynamic arrest, *Nature Mater.* **7**, 556 (2008).
- [8] C. P. Royall and S. R. Williams, The role of local structure in dynamical arrest, *Phys. Rep.* **560**, 1 (2015).
- [9] W. Dmowski, T. Iwashita, C. P. Chuang, J. Almer, and T. Egami, Elastic Heterogeneity in Metallic Glasses, *Phys. Rev. Lett.* **105**, 205502 (2010).
- [10] Y. H. Liu, D. Wang, K. Nakajima, W. Zhang, A. Hirata, T. Nishi, A. Inoue, and M. W. Chen, Characterization of Nanoscale Mechanical Heterogeneity in a Metallic Glass by Dynamic Force Microscopy, *Phys. Rev. Lett.* **106**, 125504 (2011).
- [11] H. Wagner, D. Bedorf, S. Küchemann, M. Schwabe, B. Zhang, W. Arnold, and K. Samwer, Local elastic properties of a metallic glass, *Nature Mater.* **10**, 439 (2011).
- [12] C. A. Angell, Formation of glasses from liquids and biopolymers, *Science* **267**, 1924 (1995).
- [13] L.-M. Martinez and C. A. Angell, A thermodynamic connection to the fragility of glass-forming liquids, *Nature (London)* **410**, 663 (2001).
- [14] P. Zhang, J. J. Maldonis, Z. Liu, J. Schroers, and P. M. Voyles, Spatially Heterogeneous Dynamics in a Metallic Glass Forming Liquid Imaged by Electron Correlation Microscopy, *Nat. Commun.* **9**, 1129 (2018).
- [15] A. Nicolas, E. E. Ferrero, K. Martens, and J.-L. Barrat, Deformation and flow of amorphous solids: a review of mesoscale elastoplastic models, *Rev. Mod. Phys.* **90**, 045006 (2018).
- [16] Y.-C. Hu, Y.-W. Li, Y. Yang, P.-F. Guan, H.-Y. Bai, and W.-H. Wang, Configuration correlation governs slow dynamics of supercooled metallic liquids, *Proc. Natl. Acad. Sci. U. S. A.* **115**, 6375 (2018).
- [17] L. Wang, N. Xu, W. H. Wang, and P. Guan, Universal Link between Structural Relaxation and Dynamic Heterogeneity in Glass-Forming Liquids, *Phys. Rev. Lett.* **120**, 125502 (2018).
- [18] B. Shang, J. Rottler, P. Guan, and J.-L. Barrat, Local versus Global Stretched Mechanical Response in a Supercooled Liquid near the Glass Transition, *Phys. Rev. Lett.* **122**, 105501 (2019).
- [19] Z. Wang, B. A. Sun, H. Y. Bai, and W. H. Wang, Evolution of hidden localized flow during glass-to-liquid transition in metallic glass, *Nat. Commun.* **5**, 5823 (2014).
- [20] J. C. Qiao, Y.-J. Wang, L. Z. Zhao, L. H. Dai, D. Crespo, J. M. Pelletier, L. M. Keer, and Y. Yao, Transition from stress-driven to thermally activated stress relaxation in metallic glasses, *Phys. Rev. B* **94**, 104203 (2016).

- [21] B. Cui, J. Yang, J. Qiao, M. Jiang, L. Dai, Y.-J. Wang, and A. Zaccone, Atomic theory of viscoelastic response and memory effects in metallic glasses, *Phys. Rev. B* **96**, 094203 (2017).
- [22] M. Atzmon, The pitfalls of empirical fitting of glass relaxation data with stretched exponents, *J. Appl. Phys.* **123**, 065103 (2018).
- [23] Z. W. Wu, W. Kob, W.-H. Wang, and L. Xu, Stretched and compressed exponentials in the relaxation dynamics of a metallic glass-forming melt, *Nat. Commun.* **9**, 5334 (2018).
- [24] Z. Evenson, B. Ruta, S. Hechler, M. Stolpe, E. Pineda, I. Gallino, and R. Busch, X-Ray Photon Correlation Spectroscopy Reveals Intermittent Aging Dynamics in a Metallic Glass, *Phys. Rev. Lett.* **115**, 175701 (2015).
- [25] P. Luo, P. Wen, H. Y. Bai, B. Ruta, and W. H. Wang, Relaxation Decoupling in Metallic Glasses at Low Temperatures, *Phys. Rev. Lett.* **118**, 225901 (2017).
- [26] M. Lüttich, V. M. Giordano, S. Le Floch, E. Pineda, F. Zontone, Y. Luo, K. Samwer, and B. Ruta, Anti-Aging in Ultrastable Metallic Glasses, *Phys. Rev. Lett.* **120**, 135504 (2018).
- [27] U. F. Kocks, A. S. Argon, and M. F. Ashby, Thermodynamics and kinetics of slip, *Prog. Mater. Sci.* **19**, 1 (1975).
- [28] D. Caillard and J. L. Martin, *Thermally Activated Mechanisms in Crystal Plasticity*, edited by R. W. Cahn, Pergamon Materials Series Vol. 8 (Elsevier, Oxford, 2003).
- [29] A. Castellero, B. Moser, D. I. Uhlénhaut, F. H. D. Torre, and J. F. Löffler, Room-temperature creep and structural relaxation of Mg-Cu-Y metallic glasses, *Acta Mater.* **56**, 3777 (2008).
- [30] Y.-J. Wang, J.-P. Du, S. Shinzato, L.-H. Dai, and S. Ogata, A free energy landscape perspective on the nature of collective diffusion in amorphous solids, *Acta Mater.* **157**, 165 (2018).
- [31] J. D. Ju and M. Atzmon, A comprehensive atomistic analysis of the experimental dynamic-mechanical response of a metallic glass, *Acta Mater.* **74**, 183 (2014).
- [32] T. J. Lei, L. R. Dacosta, M. Liu, W. H. Wang, Y. H. Sun, A. L. Greer, and M. Atzmon, Microscopic characterization of structural relaxation and cryogenic rejuvenation in metallic glasses, *Acta Mater.* **164**, 165 (2019).
- [33] M. Goldstein, Viscous liquids and the glass transition: A potential energy barrier picture, *J. Chem. Phys.* **51**, 3728 (1969).
- [34] F. H. Stillinger, A Topographic View Supercooled Liquids Glass Formation, *Science* **267**, 1935 (1995).
- [35] D. Wales, *Energy Landscapes: Applications to Clusters, Biomolecules and Glasses*, Cambridge Molecular Science (Cambridge University Press, Cambridge, UK, 2004).
- [36] F. H. Stillinger, *Energy Landscapes, Inherent Structures, and Condensed-Matter Phenomena* (Princeton University Press, Princeton, NJ, 2016).
- [37] L. J. Munro and D. J. Wales, Defect migration in crystalline silicon, *Phys. Rev. B* **59**, 3969 (1999).
- [38] Y. Zeng, P. H. Xiao, and G. Henkelman, Unification of algorithms for minimum mode optimization, *J. Chem. Phys.* **140**, 044115 (2014).
- [39] G. Henkelman and H. Jónsson, A dimer method for finding saddle points on high dimensional potential surfaces using only first derivatives, *J. Chem. Phys.* **111**, 7010 (1999).
- [40] W. E and X. Zhou, The gentlest ascent dynamics, *Nonlinearity* **24**, 1831 (2011).
- [41] G. T. Barkema and N. Mousseau, Event-Based Relaxation of Continuous Disordered Systems, *Phys. Rev. Lett.* **77**, 4358 (1996); R. Malek and N. Mousseau, Dynamics of lennard-jones clusters: A characterization of the activation-relaxation technique, *Phys. Rev. E* **62**, 7723 (2000); E. MacHado-Charry, L. K. Béland, D. Caliste, L. Genovese, T. Deutsch, N. Mousseau, and P. Pochet, Optimized energy landscape exploration using the ab initio based activation-relaxation technique, *J. Chem. Phys.* **135**, 034102 (2011).
- [42] D. Rodney, A. Tanguy, and D. Vandembroucq, Modeling the mechanics of amorphous solids at different length scale and time scale, *Model. Simul. Mater. Sci. Eng.* **19**, 083001 (2011).
- [43] N. Mousseau, L. K. Béland, P. Brommer, F. El-Mellouhi, J.-F. Joly, G. K. N'Tsouaglo, O. Restrepo, and M. Trochet, Following atomistic kinetics on experimental timescales with the kinetic Activation Relaxation Technique, *Comput. Mater. Sci.* **100**, 111 (2015).
- [44] D. Rodney and C. Schuh, Distribution of Thermally Activated Plastic Events in a Flowing Glass, *Phys. Rev. Lett.* **102**, 235503 (2009).
- [45] D. Rodney and C. A. Schuh, Yield stress in metallic glasses: The jamming-unjamming transition studied through Monte Carlo simulations based on the activation-relaxation technique, *Phys. Rev. B* **80**, 184203 (2009).
- [46] Y. Fan, T. Iwashita, and T. Egami, How thermally activated deformation starts in metallic glass, *Nat. Commun.* **5**, 5083 (2014).
- [47] Y. Fan, T. Iwashita, and T. Egami, Crossover from Localized to Cascade Relaxations in Metallic Glasses, *Phys. Rev. Lett.* **115**, 045501 (2015).
- [48] Y. Fan, T. Iwashita, and T. Egami, Energy landscape-driven non-equilibrium evolution of inherent structure in disordered material, *Nat. Commun.* **8**, 15417 (2017).
- [49] C. Liu, P. Guan, and Y. Fan, Correlating Defects Density in Metallic Glasses with the Distribution of Inherent Structures in Potential Energy Landscape, *Acta Mater.* **161**, 295 (2018).
- [50] J. Ding, Y. Q. Cheng, H. Sheng, M. Asta, R. O. Ritchie, and E. Ma, Universal structural parameter to quantitatively predict metallic glass properties, *Nat. Commun.* **7**, 13733 (2016).
- [51] C. E. Shannon, A mathematical theory of communication, *Bell Syst. Tech. J.* **27**, 379 (1948).
- [52] J. C. Dyre, Source of non-Arrhenius average relaxation time in glass-forming liquids, *J. Non. Cryst. Solids* **235–237**, 142 (1998).
- [53] J. C. Dyre, T. Hechsher, and K. Niss, A brief critique of the Adam-Gibbs entropy model, *J. Non. Cryst. Solids* **355**, 624 (2009).
- [54] M. I. Mendeleev, M. J. Kramer, R. T. Ott, D. J. Sordelet, D. Yagodin, and P. Popel, Development of suitable interatomic potentials for simulation of liquid and amorphous Cu-Zr alloys, *Philos. Mag.* **89**, 967 (2009).
- [55] S. Plimpton, Fast parallel algorithms for short-range molecular dynamics, *J. Comput. Phys.* **117**, 1 (1995).
- [56] M. Parrinello and A. Rahman, Polymorphic transitions in single crystals: A new molecular dynamics method, *J. Appl. Phys.* **52**, 7182 (1981).
- [57] S. Nosé, A unified formulation of the constant temperature molecular dynamics methods, *J. Chem. Phys.* **81**, 511 (1984); W. G. Hoover, Canonical dynamics: Equilibrium phase-space distributions, *Phys. Rev. A* **31**, 1695 (1985).
- [58] E. Cancès, F. Legoll, M. C. Marinica, K. Minoukadeh, and F. Willaime, Some improvements of the activation-relaxation

- technique method for finding transition pathways on potential energy surfaces, *J. Chem. Phys.* **130**, 114711 (2009).
- [59] D. Wei, J. Yang, M. Q. Jiang, B. C. Wei, Y. J. Wang, and L. H. Dai, Revisiting the structure-property relationship of metallic glasses: Common spatial correlation revealed as a hidden rule, *Phys. Rev. B* **99**, 014115 (2019).
- [60] H. L. Smith, C. W. Li, A. Hoff, G. R. Garrett, D. S. Kim, F. C. Yang, M. S. Lucas, T. Swan-Wood, J. Y. Y. Lin, M. B. Stone, D. L. Abernathy, M. D. Demetriou, and B. Fultz, Separating the configurational and vibrational entropy contributions in metallic glasses, *Nat. Phys.* **13**, 900 (2017).
- [61] T. Wang, T. E. Cullinan, and R. E. Napolitano, A new method for measuring the thermodynamic properties of undercooled liquid and amorphous Cu-Zr alloys, *Acta Mater.* **62**, 188 (2014).
- [62] H. B. Yu, K. Samwer, Y. Wu, and W. H. Wang, Correlation between  $\beta$  Relaxation and Self-Diffusion of the Smallest Constituting Atoms in Metallic Glasses, *Phys. Rev. Lett.* **109**, 095508 (2012).
- [63] H. B. Yu, M. Tylinski, A. Guiseppi-Elie, M. D. Ediger, and R. Richert, Suppression of  $\beta$  Relaxation in Vapor-Deposited Ultrastable Glasses, *Phys. Rev. Lett.* **115**, 185501 (2015).
- [64] A. S. Argon, Plastic deformation in metallic glasses, *Acta Metall.* **27**, 47 (1979).
- [65] M. L. Falk and J. S. Langer, Dynamics of viscoplastic deformation in amorphous solids, *Phys. Rev. E* **57**, 7192 (1998).
- [66] P. M. Derlet and R. Maaß, Linking high and low temperature plasticity in bulk metallic glasses: thermal activation, extreme value statistics and kinetic freezing, *Philos. Mag.* **93**, 4232 (2013).
- [67] P. Derlet and R. Maaß, Linking high- and low-temperature plasticity in bulk metallic glasses II: use of a log-normal barrier energy distribution and a mean-field description of high-temperature plasticity, *Philos. Mag.* **94**, 2776 (2014).
- [68] W. L. Johnson and K. Samwer, A Universal Criterion for Plastic Yielding of Metallic Glasses with a  $(T/T_g)^{2/3}$  Temperature Dependence, *Phys. Rev. Lett.* **95**, 195501 (2005).
- [69] H. Tong and H. Tanaka, Revealing Hidden Structural Order Controlling Both Fast and Slow Glassy Dynamics in Supercooled Liquids, *Phys. Rev. X* **8**, 011041 (2018).
- [70] E. D. Cubuk, R. J. S. Ivancic, S. S. Schoenholz, D. J. Strickland, A. Basu, Z. S. Davidson, J. Fontaine, J. L. Hor, Y.-R. Huang, Y. Jiang, N. C. Keim, K. D. Koshigan, J. A. Lefever, T. Liu, X.-G. Ma, D. J. Magagnosc, E. Morrow, C. P. Ortiz, J. M. Rieser, A. Shavit, T. Still, Y. Xu, Y. Zhang, K. N. Nordstrom, P. E. Arratia, R. W. Carpick, D. J. Durian, Z. Fakhraai, D. J. Jerolmack, D. Lee, J. Li, R. Riggleman, K. T. Turner, A. G. Yodh, D. S. Gianola, and A. J. Liu, Structure-property relationships from universal signatures of plasticity in disordered solids, *Science* **358**, 1033 (2017).
- [71] V. K. de Souza, J. D. Stevenson, S. P. Niblett, J. D. Farrel, and D. J. Wales, Defining and quantifying frustration in the energy landscape: Applications to atomic and molecular clusters, biomolecules, jammed and glassy systems, *J. Chem. Phys.* **146**, 124103 (2017).
- [72] D. J. Wales, Exploring energy landscapes, *Annu. Rev. Phys. Chem.* **69**, 401 (2018).
- [73] D. Wei, J. Yang, M. Q. Jiang, L. H. Dai, Y. J. Wang, J. C. Dyre, I. Douglass, and P. Harrowell, Assessing the utility of structure in amorphous materials, *J. Chem. Phys.* **150**, 114502 (2019).
- [74] S. Sastry, The relationship between fragility, configurational entropy and the potential energy landscape of glass-forming liquids, *Nature (London)* **409**, 164 (2001).
- [75] B. Doliwa and A. Heuer, Hopping in a supercooled Lennard-Jones liquid: Metabasins, waiting time distribution, and diffusion, *Phys. Rev. E* **67**, 030501(R) (2003).
- [76] A. Saksengwijit, B. Doliwa, and A. Heuer, Description of the dynamics in complex energy landscapes via metabasins: A simple model study, *J. Phys.: Condens. Matter* **15**, S1237 (2003).
- [77] T. F. Middleton and D. J. Wales, Energy landscapes of model glasses. II. Results for constant pressure, *J. Chem. Phys.* **118**, 4583 (2003).
- [78] V. K. de Souza and D. J. Wales, Energy landscapes for diffusion: Analysis of cage-breaking processes, *J. Chem. Phys.* **129**, 164507 (2008).
- [79] S. P. Niblett, V. K. de Souza, J. D. Stevenson, and D. J. Wales, Dynamics of a molecular glass former: Energy landscapes for diffusion in ortho-terphenyl, *J. Chem. Phys.* **145**, 024505 (2016).
- [80] N. Lempeis, G. C. Boulougouris, and D. N. Theodorou, Temporal disconnectivity of the energy landscape in glassy systems, *J. Chem. Phys.* **138**, 12A545 (2013).
- [81] O. M. Becker and M. Karplus, The topology of multidimensional potential energy surfaces: Theory and application to peptide structure and kinetics, *J. Chem. Phys.* **106**, 1495 (1997).
- [82] D. J. Wales, Energy landscapes: Calculating pathways and rates, *Int. Rev. Phys. Chem.* **25**, 237 (2006).
- [83] S. P. Niblett, M. Biedermann, D. J. Wales and V. K. de Souza, Pathways for diffusion in the potential energy landscape of the network glass former SiO<sub>2</sub>, *J. Chem. Phys.* **147**, 152726 (2017).
- [84] A. Kushima, X. Lin, J. Li, J. Eapen, J. C. Mauro, X. F. Qian, P. Diep, and S. Yip, Computing the viscosity of supercooled liquids, *J. Chem. Phys.* **130**, 224504 (2009).
- [85] A. Kushima, X. Lin, J. Li, J. Eapen, J. C. Mauro, X. F. Qian, P. Diep, and S. Yip, Computing the viscosity of supercooled liquids. II. Silica and strong-fragile crossover behavior, *J. Chem. Phys.* **131**, 164505 (2009).
- [86] V. K. de Souza and D. J. Wales, Connectivity in the potential energy landscape for binary Lennard-Jones systems, *J. Chem. Phys.* **130**, 014115 (2009).
- [87] T. F. Middleton and D. J. Wales, Energy landscapes of some model glass formers, *Phys. Rev. B* **64**, 024205 (2001).
- [88] J. C. Mauro, R. J. Loucks, J. Balakrishnan, and A. K. Varshneya, Potential energy landscapes of elemental and heterogeneous chalcogen clusters, *Phys. Rev. A* **73**, 023202 (2006).
- [89] D. J. Wales, M. A. Miller, and T. R. Walsh, Archetypal energy landscapes, *Nature (London)* **394**, 758 (1998).
- [90] H. Tanaka, H. Tong, R. Shi, and J. Russo, Revealing key structural features hidden in liquids and glasses, *Nat. Rev. Phys.* **1**, 333 (2019).
- [91] H. W. Sheng, W. K. Luo, F. M. Alamgir, J. M. Bai, and E. Ma, Atomic packing and short-to-medium-range order in metallic glasses, *Nature (London)* **439**, 419 (2006).

- [92] Y. Cheng and E. Ma, Atomic-level structure and structure-property relationship in metallic glasses, *Prog. Mater. Sci.* **56**, 379 (2010).
- [93] J. Ding, S. Patinet, M. L. Falk, Y. Cheng, and E. Ma, Soft spots and their structural signature in a metallic glass, *Proc. Natl. Acad. Sci. U.S.A.* **111**, 14052 (2014).
- [94] W. Kauzmann, The Nature of the Glassy State and the Behavior of Liquids at Low Temperatures, *Chem. Rev.* **43**, 219 (1948).
- [95] G. Adam and J. H. Gibbs, On the temperature dependence of cooperative relaxation properties in glass-forming liquids, *J. Chem. Phys.* **43**, 139 (1965).
- [96] D. Han, D. Wei, J. Yang, H.-L. Li, M.-Q. Jiang, Y.-J. Wang, L.-H. Dai, and A. Zaccane, Atomistic structural mechanism for the glass transition: Entropic contribution, *Phys. Rev. B* **101**, 014113 (2020).